Article ID: 1006-8775(2018) 01-0001-14

THE RELATIONSHIP BETWEEN HORIZONTAL VORTICITY INDUCED BY VERTICAL SHEAR AND VERTICAL MOTION DURING A SQUALL LINE PROCESS

ZHAO Xiang-jun (赵向军)[1, 2], DING Zhi-ying (丁治英)[1]
(1. Nanjing University of Information Science and Technology/Key Laboratory of Meteorological Disaster co-funded by Ministry of Education and Jiangsu Province, Jiangsu Nanjing 210044 China;
2. State Key Laboratory of Severe Weather, Chinese Academy of Meteorological of Sciences, Beijing 100081 China)

Abstract: The horizontal vorticity equation used in this study was obtained using the equations of motion in the pressure coordinate system without considering friction, to reveal its relationship with vertical shear. By diagnostically analyzing each term in the horizontal vorticity equation during a squall line process that occurred on 19 June 2010, we found that the non-thermal wind term had a negative contribution to the local change of upward movement in the low-level atmosphere, and that its impact changed gradually from negative to positive with altitude, which could influence upward movement in the mid- and upper-level atmosphere greatly. The contribution of upward vertical transport to vertical movement was the largest in the low-level atmosphere, but had negative contribution to the upper-level atmosphere. These features were most evident in the development stage of the squall line. Based on analysis of convection cells along a squall line, we found that in the process of cell development diabatic heating caused the subsidence of constant potential temperature surface and non-geostrophic motion, which then triggered strong convergence of horizontal acceleration in the mid-level atmosphere and divergence of horizontal acceleration in the upper-level atmosphere. These changes of horizontal wind field could cause a counterclockwise increment of the horizontal vorticity around the warm cell, which then generated an increase of upward movement. This was the main reason why the non-thermal wind term had the largest contribution to the strengthening of upward movement in the mid- and upper-level atmosphere. The vertical transport of large value of horizontal vorticity was the key to trigger convection in this squall line process.

Key words: horizontal vorticity; horizontal vorticity equation; vorticity of horizontal vorticity; squall line; non-thermal wind
CLC number: P458.2 **Document code:** A
doi: 10.16555/j.1006-8775.2018.01.001

1 INTRODUCTION

In the mid-latitude region, a squall line is one of the most common mesoscale convective systems. It often causes disastrous convective weathers, such as regional rainstorm, short-term gusty wind and hail.

The low-level vertical wind shear generated by weather system or circulation pattern is the most important boundary layer characteristics for the development and maintenance of a squall line. In the early 1950s and 1960s, Newton, Fujita and Ludlam concluded from their research that the scale of the ambient vertical wind shear perpendicular to the squall line is the key factor for squall line development [1-4]. They were the first to develop the conceptual model for studying the impact of vertical wind shear on windstorm, and they proposed a two-dimensional (2D) structure in which the storm characteristics are kept unchanged along the squall line (i.e., the development characteristics are the same for all storm cells along the squall line). Thorpe et al. [20] further showed that the low-level ambient vertical wind shear is a necessary characteristic affecting the maintenance of a squall line; and if there is strong enough low-level shear perpendicular to the squall line, it can prevent the windstorm outflow (i.e., gust front) from moving forward fast to maintain the ceaseless rising of the low-level vertical airflow and form favorable conditions for sustaining the development of the storm cells within the squall line. They successfully simulated and verified the 2D squall line conceptual model proposed by

Received 2017-03-02; **Revised** 2017-11-30; **Accepted** 2018-02-15
Foundation item: National Key Basic Research Development Program "973"(2013CB430103); State Key Laboratory of Severe Weather, Chinese Academy of Meteorological Sciences (2015LASW-A07); National Natural Science Funding (41375058, 41530427)
Biography: DING Zhi-ying, Professor, primarily undertaking research on mesoscale meteorology.
Corresponding author: DING Zhi-ying, e-mail: dingzhiying@nuist.edu.cn

Newton, Fujita and Ludlam. Observational analyses also showed that both strong and weak squall lines are characterized by significant low-level vertical wind shear and that a stronger low-level shear perpendicular to the squall line will result in a stronger squall line and a longer life cycle (Bluestein, et al.[5,6]). After analyzing the existing observation and research results, Rotunno et al. and Weisman et al. used idealized numerical experiments of 2D and 3D cloud models, respectively, to put forward for the first time that the interaction between the near-surface cold pool and the low-level ambient vertical wind shear is the most important dynamic and thermodynamic mechanisms for the development and maintenance of a squall line, thus forming the "RKW" theory describing the development and propagation of a squall line [7, 8]. The RKW theory states that the interaction between the cold pool and the low-level vertical wind shear is closely related to the height of vertical rising and vertical velocity of the airflow at the front of a squall line, acting as the most important influence factor at the front of the squall line to constantly trigger new convection cells. Weisman et al. and Bryan et al. confirmed that the RKW theory was reasonable both qualitatively and quantitatively, for describing the development and maintenance of a squall line and its life cycle characteristics [9-11]. Ding et al. revealed the relationship between vertical wind shear and vertical movement in the form of horizontal vorticity, pointing out that the counterclockwise rotation of horizontal vorticity corresponds to upward movement while the clockwise rotation of horizontal vorticity corresponds to downward motion[12]. They estimated the size of vertical movement using a relaxation method and iteration. Their results showed that the vertical movement calculated based on this method is extremely close to that from the WRF (Weather Research and Forecasting Model).

As mentioned above, vertical wind shear plays an important role in the development of a squall line, which has been recognized by many researchers. However, which factors influence the change of vertical wind shear in the evolution of a squall line? What is the difference between the influence of upper-level vertical shear and that of low-level vertical shear for the vertical movement along a squall line? We carry out detailed analysis to answer these questions, using a numerical simulation of a strong squall line process that occurred in June 2010 over southern China.

The remainder of this paper is organized as follows. We summarize the evolution of the squall line in section 2. An overview of the data and model validation is given in section 3. The relationship between horizontal vorticity induced by vertical wind shear and vertical velocity is given in section 4. We show the distribution of each term on the right hand side of the horizontal vorticity equation during the development of the squall line in section 5; and we also analyze the mechanism at work. Finally, summary and discussion are given in section 6.

2 AN OVERVIEW OF THE SQUALL LINE AND ITS ENVIRONMENT

At 0900 UTC 19 June 2010, a squall line appeared at the boundary of southeastern Guizhou province and northwestern Guangxi region, with multiple convection cells (Fig.1a & 1b). The convection cells started to develop toward the northeastern region. After 1000 UTC, the convective clouds in the northeast became weaker gradually, while the convective clouds in the southwest developed further and extended to the west and also obviously to the south. At 1200 UTC (Fig.1d), the convection line showed obvious development to the southwest. At 1400—1500 UTC (Fig.1f & 1g), the strong convection area began to appear on the edge of the southern region, with stratiform clouds widening at the rear of the squall line. At 1530 UTC (Fig.1h), the squall line showed its typical bow echo. At 1600 UTC, the echo reached its peak and then the squall line started to weaken. At 1900 UTC, the strong echo disappeared (not shown).

Table 1 shows the convective available potential energy (CAPE) of each sounding station at 0000 UTC 19 June before the occurrence of the squall line; the stations are located from central Guizhou to southern Guangxi. Observational analyses(Bluestein et al.; Parker et al.[13]; Weckwerth[14]; Romanski and B.rossow[15]; Peng et al.[16]) pointed out that the larger the CAPE is, the better for the environmental thermal uplift condition for the generation of new windstorm cells and thus more beneficial for the maintenance of the whole squall line system. For the development of a squall line, CAPE may have a large range. In general, when the CAPE is about 1,000 J/kg, it is favorable for forming a squall line system of average strength; but when the CAPE is larger than 2,200 J/kg, a stronger squall line system may come into being. As can be seen from the table, before the squall line occurred at each station, there was high CAPE; especially in northwest, northern and southern Guangxi, where more mature development of the squall line occurred and the maximum CAPE reached 3,173.4 J/kg. Therefore, the CAPE in the surrounding environment was favorable for the development of the squall line.

As can be seen from the 6-hourly, 1° × 1° final analysis (FNL) data, provided by the National Centers for Environmental Prediction (NCEP), the process of the squall line from formation, development, maturity to disappearance was accompanied by eastward movement of the shear line and the southwest vortex. At 0000 UTC 19 June, the vortex center located to the northwest of Guizhou was characterized by the wind shear between northwesterly and southwesterly (Fig.2a), as shown by the blue line AB in Fig.2. With the eastward movement of the southwest vortex, the shear line AB

moved from northwest to southeast of Guizhou after 0000 UTC 19 June and eventually into northern Guangxi. The western part of the shear line was strengthened (Fig.2b-d) and consistent with the squall line in terms of orientation and movement direction. At the rear of the shear line, there was a sharp equivalent potential temperature gradient, which suggests that the squall line was accompanied by a cold front.

Table 1. Convective available potential energy and 0—3 km wind shear of each sounding station at 0000 UTC.

Station	Site location	Convective available potential energy (units: J·kg^{-1})	0—3 km vertical shear (units: m/s)
Guiyang	Central Guizhou	1687.0	17.5
Guilin	Northeastern Guangxi	1894.8	13
Hechi	Northern Guangxi	2332.5	10
Baise	Northwestern Guangxi	3173.4	10

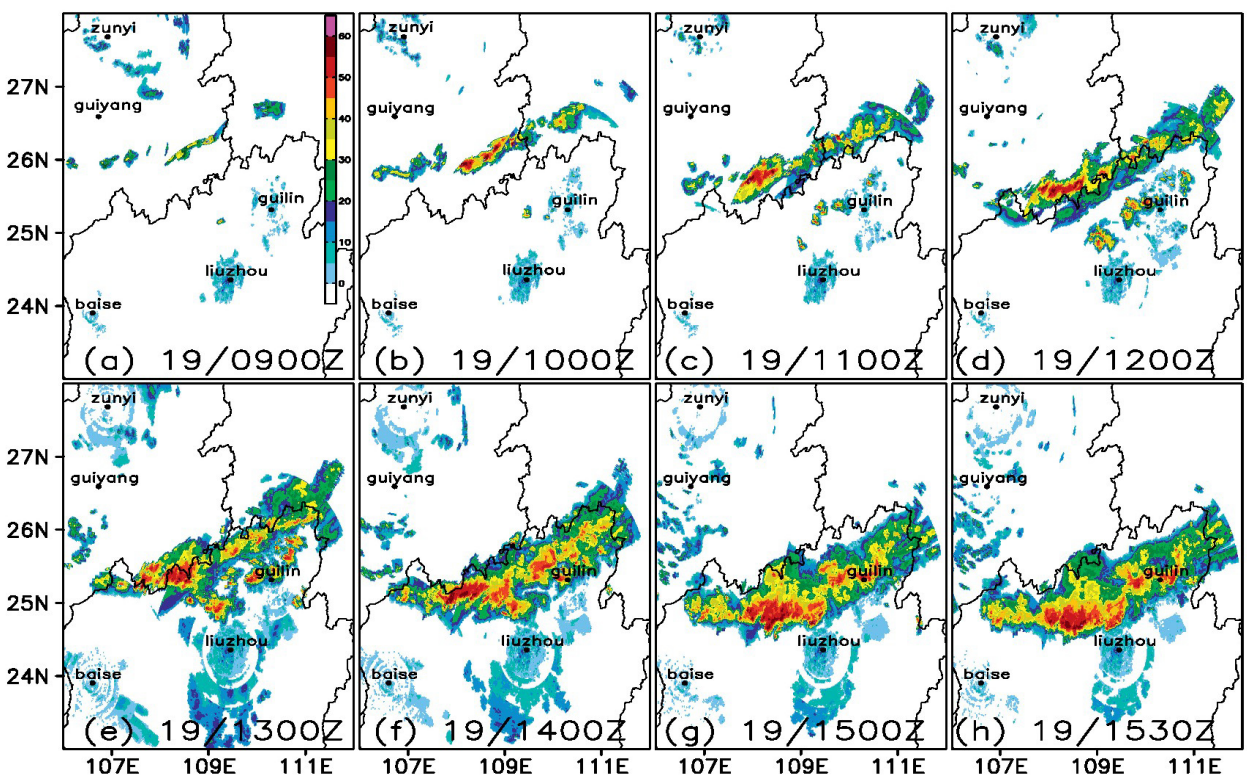

Figure 1. Observed squall line evolution at 700 hPa. shading indicates composite reflectivity (dBZ). The radar stations of Zunyi, Guiyang, Guilin, Liuzhou and Baise are indicated by black dots.

3 DATA AND MODEL VALIDATION

In this study, the process of the squall line was numerically simulated using the mesoscale model WRFV3.3, which was jointly developed by the NCEP and the National Center for Atmospheric Research (NCAR). The initial fields and boundary conditions are from the 6-hourly NCEP FNL data at the resolution of 1°×1°. The physical schemes adopted mainly include Lin microphysical scheme (Lin et al [17]), Yonsei State University (YSU) boundary layer scheme (Noh et al.[18]), Kain-Fritsch cumulus parameterization scheme, Noah land surface process scheme, RRTM longwave radiation, and Dudhia shortwave radiation scheme. The model uses the three-layered two-way nesting, with horizontal resolutions of 36, 12 and 4 km, respectively. There are 28 vertical levels. The model integration started at 0000 UTC 19 June, and ended at 1200 UTC 20 June, over a period of 36 hours. In this paper, the outputs from the fine grid (4 km) with the time interval of 10 minutes are analyzed.

The comparison between the observed and simulated radar echo demonstrates that although the simulated echo are located further south than the observed (Fig.3), the orientation of simulated echo agrees well with the observation, oriented along the northeast-southwest direction. The evolution of the simulated echo agrees well with that of the observed:

developing westward and moving simultaneously southward after 1000 UTC. A bow-shaped echo appeared around 1600 UTC. The strengths of the multiple strong echo centers of the simulated echo belt are also consistent with those of the radar observations, but the simulated echo for the stratiform clouds cover a smaller area than the observed. In summary, these model outputs are adequate for further analysis.

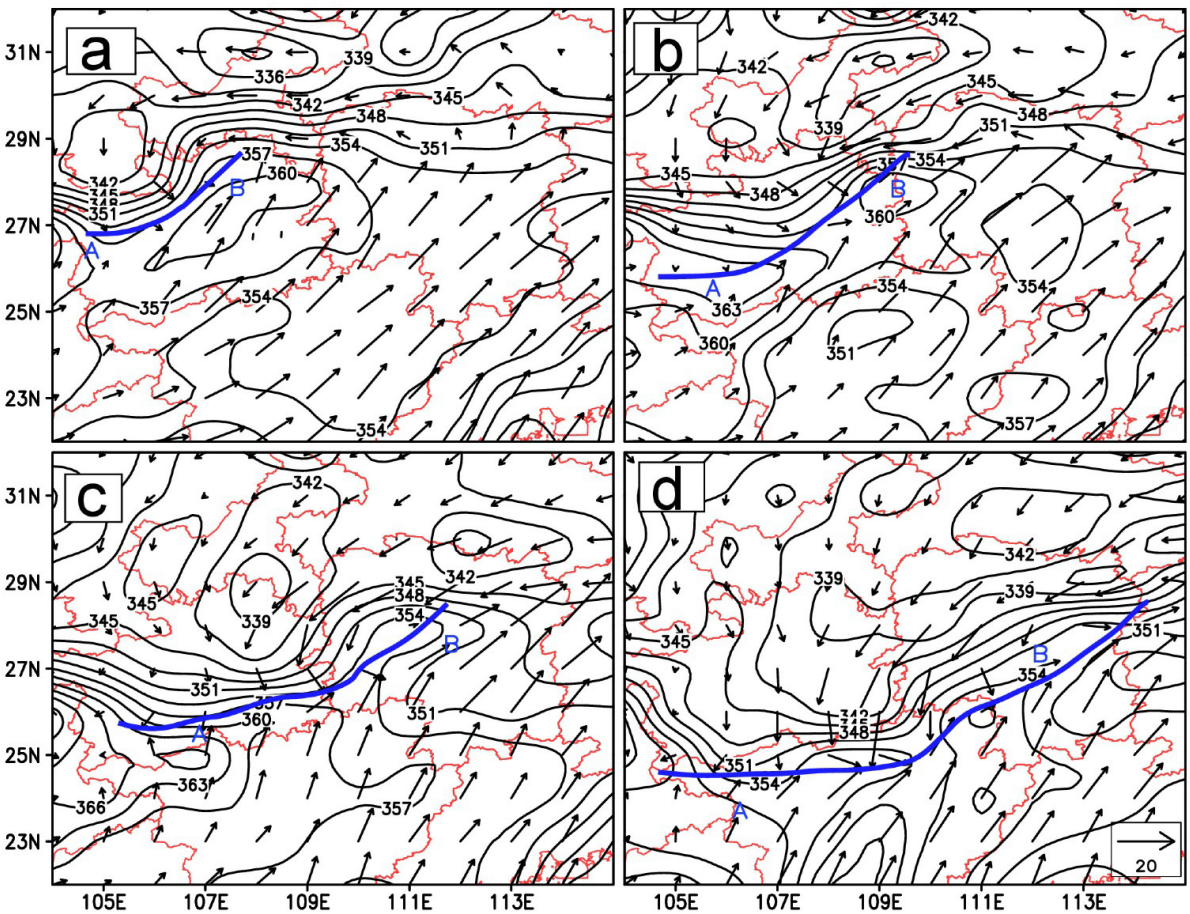

Figure 2. (a)-(d): The locations of the southwest vortex and the shear line (blue solid line) at 850 hPa from 0000 to 1800 UTC 19 June according to the NCEP FNL data (time interval: 6-hourly). black solid line: equivalent potential temperature (k); vector: wind field ($m \cdot s^{-1}$).

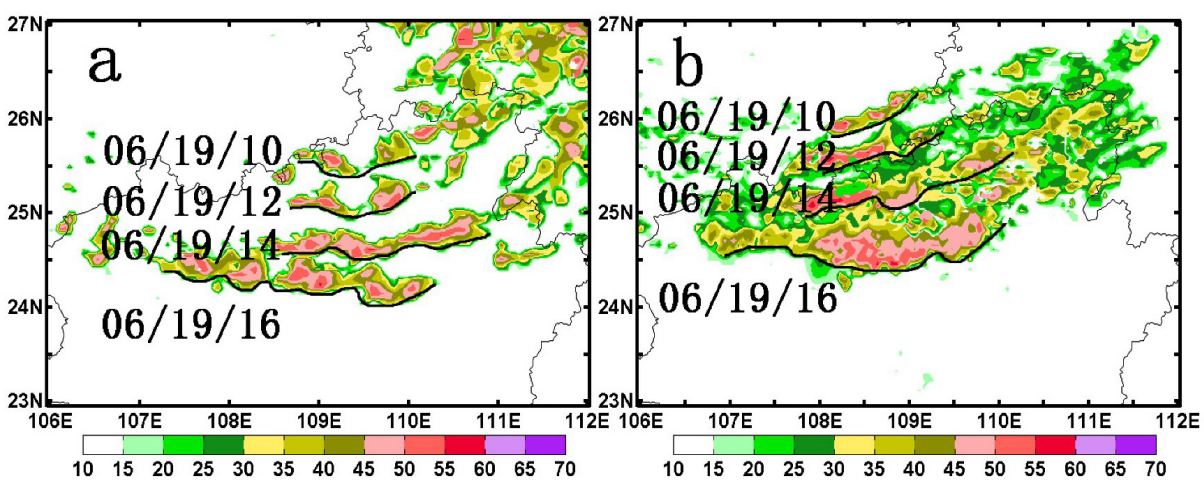

Figure 3. (a) Distribution of simulated echo from 1000 to 1600 UTC 19 June 2010; (b) Distribution of observed radar echo from 1000 to 1600 UTC 19 June 2010. Units: dBZ.

4 RELATIONSHIP BETWEEN HORIZONTAL VORTICITY AND VERTICAL VELOCITY

By taking derivative on P at both sides of the continuity equation, Ding et al. obtained the Poisson equation as follows:

$$\frac{\partial}{\partial x}\left(-\frac{\partial u}{\partial p}\right)-\frac{\partial}{\partial y}\left(\frac{\partial v}{\partial p}\right)=\frac{\partial^2\omega}{\partial p^2} \tag{1}$$

$$vhv=\frac{\partial\xi_y}{\partial x}-\frac{\partial\xi_x}{\partial y}=\frac{\partial}{\partial x}\left(-\frac{\partial u}{\partial p}\right)-\frac{\partial}{\partial y}\left(\frac{\partial v}{\partial p}\right)$$

In Eq.(1), $\left(\frac{\partial v}{\partial p},-\frac{\partial u}{\partial p}\right)=(\xi_x,\xi_y)$ is the horizontal vorticity induced by vertical shear (hereinafter referred to as horizontal vorticity). vhv is the vorticity of horizontal vorticity, representing the rotation of the horizontal vorticity induced by vertical shear in the horizontal direction. For convenience, the vorticity of horizontal vorticity is referred as vhv from now on. Using the Richardson relaxation iterative method, Ding et al. solved for the vertical velocity using Eq.(1). By comparing with the vertical velocity of the WRF output and the vertical velocity calculated by the kinematic method, the usefulness of Eq.(1) is verified. When ω is perturbed, $\frac{\partial^2\omega}{\partial p^2}<-\omega$ (Zhu et al.[19]). Therefore, $vhv=\frac{\partial}{\partial x}\left(-\frac{\partial u}{\partial p}\right)-\frac{\partial}{\partial y}\left(\frac{\partial v}{\partial p}\right)<-\omega$ can be obtained from (1). Further, Ding et al. concluded that when the horizontal vorticity vector $\left(\frac{\partial v}{\partial p},\frac{\partial u}{\partial p}\right)$ rotates clockwise, $vhv<0$, and then we have $\omega>0$, accompanying the occurrence of a downdraft. When the horizontal vorticity vector rotates counterclockwise, $vhv>0$, and then we have $\omega<0$, accompanying the occurrence of an updraft. Both cases are shown in Fig.4. A similar rotation can be formed around the vertical movement for the other component $\left(\frac{\partial w}{\partial y},-\frac{\partial w}{\partial x}\right)$ of the horizontal vorticity.

Ding et al. proposed not only the relationship between the rotation direction of horizontal vorticity and the direction of vertical movement but also showed the quantitative relationship between the horizontal vorticity induced by vertical shear and vertical movement. We hope to further reveal the relationship between the local change of horizontal vorticity and the local change of vertical movement in this study, to find out which factors play key roles in the local change of horizontal vorticity or the local change of vertical movement.

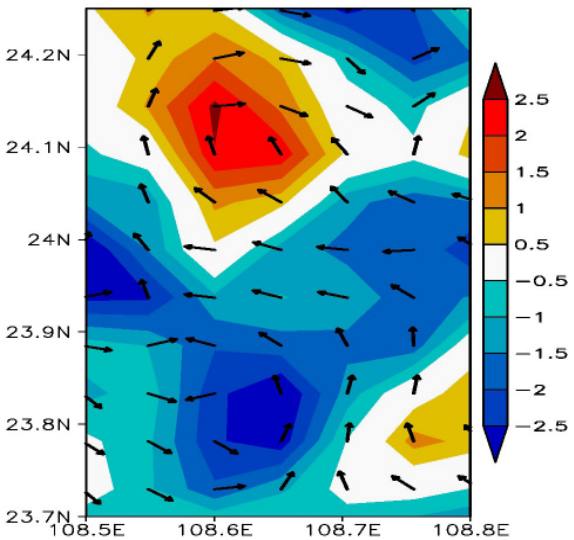

Figure 4. Horizontal vorticity of $\left(\frac{\partial v}{\partial p},-\frac{\partial u}{\partial p}\right)$ at 200 hPa (units: 10^{-3} m s^{-1} pa^{-1}). Shading represents vertical velocity (units: Pa s^{-1}).

4.1 *Equation for the local change of horizontal vorticity*

Without considering friction, Eqs.(2) and (3) are the equations of motion in the pressure coordinate system.

$$\frac{\partial v}{\partial t}+u\frac{\partial v}{\partial x}+v\frac{\partial v}{\partial y}+\omega\frac{\partial v}{\partial p}=-\frac{\partial\Phi}{\partial y}-fu \tag{2}$$

$$\frac{\partial u}{\partial t}+u\frac{\partial u}{\partial x}+v\frac{\partial u}{\partial y}+\omega\frac{\partial u}{\partial p}=-\frac{\partial\Phi}{\partial x}+fv \tag{3}$$

where f and Φ are the geostrophic parameter and geopotential field, respectively.

Taking partial derivative of Eq.(2) with respect to p and using the continuity equation, we can obtain

$$\begin{aligned}\frac{\partial\xi_x}{\partial t}&=\frac{\partial}{\partial t}\left(\frac{\partial v}{\partial p}\right)=-\left(\frac{\partial^2\Phi}{\partial p\partial y}+f\frac{\partial u}{\partial p}\right)-\left(u\frac{\partial\xi_x}{\partial x}+v\frac{\partial\xi_y}{\partial y}\right)-\omega\frac{\partial\xi_x}{\partial p}-\left(\frac{\partial u}{\partial p}\frac{\partial v}{\partial x}+\frac{\partial v}{\partial p}\frac{\partial v}{\partial y}+\frac{\partial\omega}{\partial p}\frac{\partial v}{\partial p}\right)\\&=-f\left(\frac{\partial u}{\partial p}+\frac{1}{f}\frac{\partial^2\Phi}{\partial p\partial y}\right)-\left(u\frac{\partial\xi_x}{\partial x}+v\frac{\partial\xi_x}{\partial y}\right)-\omega\frac{\partial\xi_x}{\partial p}-\left(\frac{\partial u}{\partial p}\frac{\partial v}{\partial x}+\frac{\partial v}{\partial p}\frac{\partial v}{\partial y}+\frac{\partial\omega}{\partial p}\frac{\partial v}{\partial p}\right)\\&=-f\frac{\partial}{\partial p}(u-u_g)-\left(u\frac{\partial\xi_x}{\partial x}+v\frac{\partial\xi_x}{\partial y}\right)-\omega\frac{\partial\xi_x}{\partial p}+\left(-\frac{\partial v}{\partial x}\frac{\partial u}{\partial p}+\frac{\partial u}{\partial x}\frac{\partial v}{\partial p}\right)\end{aligned} \tag{4}$$

Taking partial derivative of Eq.(3) similarly will give us the following result:

$$\frac{\partial\xi_y}{\partial t}=-f\frac{\partial}{\partial p}(v-v_g)-\left(u\frac{\partial\xi_y}{\partial x}+v\frac{\partial\xi_y}{\partial y}\right)-\omega\frac{\partial\xi_y}{\partial p}+\frac{\partial v}{\partial p}\frac{\partial u}{\partial y}-\frac{\partial u}{\partial p}\frac{\partial v}{\partial y} \tag{5}$$

The terms ranging from left to right on the right hand side of the horizontal vorticity equation are as follows: non-thermal wind, horizontal vorticity advection, horizontal vorticity vertical transport and twisting and the divergence term. Here, the non-thermal winds is the change of ageostrophic winds with height. The twisting term is the result of vertical vorticity being converted to horizontal vorticity. The divergence term is

the change of the horizontal vorticity caused by divergence/convergence of horizontal vorticity.

4.2 *Wind field and wind speed at different elevations*

Since the two above-mentioned equations can be regarded as changes of the two components of the horizontal vorticity vector, they can be seen as two vector components in the horizontal direction. If we solved the vertical vorticity at both sides of the equation, the left hand side will constitute the change of the vorticity over time for the horizontal vorticity vector rotating in the horizontal direction (hereafter referred to as vlocc). For example, the left hand side term of the equation can be written as follows:

$$\frac{\partial}{\partial x}\frac{\partial \xi_y}{\partial t}-\frac{\partial}{\partial y}\frac{\partial \xi_x}{\partial t}=\frac{\partial}{\partial t}\left(\frac{\partial \xi_y}{\partial x}-\frac{\partial \xi_x}{\partial y}\right)$$

Assume the existence of a wave solution, take partial derivative of Eq.(1) with respect to t and we can also obtain

$$\frac{\partial}{\partial t}\left(\frac{\partial \xi_y}{\partial x}-\frac{\partial \xi_x}{\partial y}\right)=\frac{\partial}{\partial t}\frac{\partial^2 \omega}{\partial p^2}\prec-\frac{\partial \omega}{\partial t}\prec\frac{\partial w}{\partial t} \qquad (6)$$

Therefore, we obtain the relationship between the equation and the local change of vertical movement. Similarly, solving for vertical vorticity using each term on the right hand side of the equation can show the relative contribution to the local change of vertical velocity in the horizontal vorticity equation. For convenience, A, B, C, D, and E are used, respectively, to represent the vertical vorticity from the non-thermal wind term, horizontal vorticity advection term, horizontal vorticity vertical transport term, divergence term, and twisting term on the right hand sides of Eqs. (4) and (5). The sum is the total of the above terms. The left hand side terms in Eqs.(4) and (5), namely, the local changes of horizontal vorticity, are referred to as vlocc, as we did for Eq. (6). In this way, we can establish the relationship between local change of horizontal vorticity rotating in the horizontal direction and local change of vertical velocity; that is to say, each term on the right hand side of the equation is directly proportional to $-\frac{\partial \omega}{\partial t}$. And when each term on the right hand side is greater than zero, it is conducive to the development of upward movement. When each term on the right hand side is smaller than zero, it is advantageous to the development of sinking motion. How each term on the right hand side of the equation contributes to local change of vertical velocity will be discussed in the next section.

5 DIAGNOSTIC ANALYSIS OF THE HORIZONTAL VORTICITY EQUATION DURING THE EVOLUTION OF THE SQUALL LINE

5.1 *Distribution of each term on the right hand side of the horizontal vorticity equation in the development of the squall line*

The analysis so far has shown that the local change of vertical movement is related to the vorticity of each term on the right hand sides of Eqs.(4) and (5). Since vorticity reflects the horizontal rotation of a vector, we will show the rotation of the first three terms on the right hand sides of Eqs.(4) and (5) in the high-, mid- and low-level atmosphere at 1400 UTC 19 June 2010.

In Fig.5a, the non-thermal wind vector in the 200-hPa strong convection zone shows obvious counterclockwise rotation; its vorticity was positive, which was advantageous to the strengthening of upward movement. The vertical transport vector shows obvious clockwise rotation (Fig.5b); its vorticity was negative, which was not conducive to the strengthening of upward movement. The horizontal advection vector in the upward movement zone mostly shows clockwise rotation, but more slowly (Fig.5c). Compared with 200 hPa, the 500-hPa non-thermal wind term was characterized by the same but weaker rotation, while the rotations of the vertical transport and advection terms were not as obvious as those in the upper-level atmosphere, except for it being weaker (Figs.5a1-c1). The analysis of each term at 800 hPa shows that the rotation in the low-level atmosphere was not obvious; and compared with 200 hPa, the vectors were relatively smaller (Figs.5a2-c2). Fig.5a1 & 5b1 show that the non-thermal wind vector was opposite to the vertical transport vector in direction, which indicates that they might contribute to the local change of vertical movement in the low-level atmosphere in opposite ways.

In both upper- and lower-level atmosphere, the twisting and divergence vectors were much smaller than the non-thermal wind, vertical transport and horizontal advection vectors (not shown). Moreover, in the upper-level atmosphere the twisting and divergence items were characterized by little rotation. Therefore, the twisting and divergence items contributed far less to the local change of vertical movement than the other three terms, and the contributions by the twisting and divergence items could be ignored.

5.2 *Qualitative analysis of each term in the horizontal vorticity equation for its contribution to vertical motion*

Figure 6 shows the average vertical velocity time evolution in the 800-hPa squall line area. The black line is the time evolution of the average vertical velocity of updraft. The blue line is the time evolution of the average vertical velocity of downdraft. As can be seen from the figure, in the squall line formation stage (0900–1050 UTC) the updraft and downdraft intensity is weak. In the squall line development and maturation stage (1100–1550 UTC) the updraft and downdraft intensity has a significant increase, the maximum average vertical velocity reached $1\mathrm{m\cdot s^{-1}}$ and $-0.8\mathrm{m\cdot s^{-1}}$. The intensity of the vertical motion at the dissipation phase (1600-1750 UTC) of the squall line decreases rapidly. It can be seen from the above analysis that the

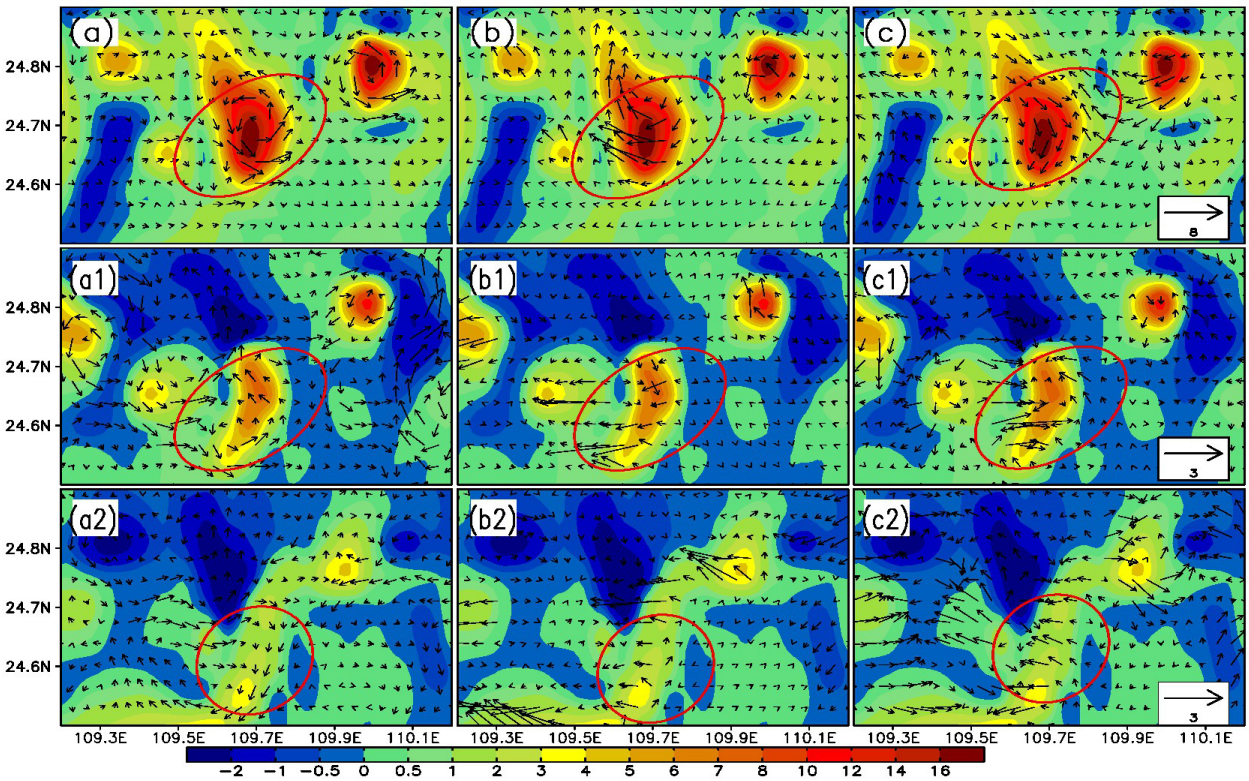

Figure 5. Maps at 1400 UTC 19 June 2010. (a)-(c): 200-hPa non-thermal wind, vertical transport and horizontal advection vectors (arrows) and the vertical motion on the right hand sides of Eqs.(4) and (5) (shading; units: m·s^{-1}). (a1)-(c1): Same as (a)-(c), except for 500 hPa. (a2)-(c2): Same as (a)-(c), except for 800 hPa.

intensity of the vertical motion at each stage of the development of the squall line has a good correspondence with the evolution of the squall line. Therefore, it is important to grasp the relationship between each term on the right side of the horizontal vorticity equation and the vertical motion to predict the evolution of the squall line.

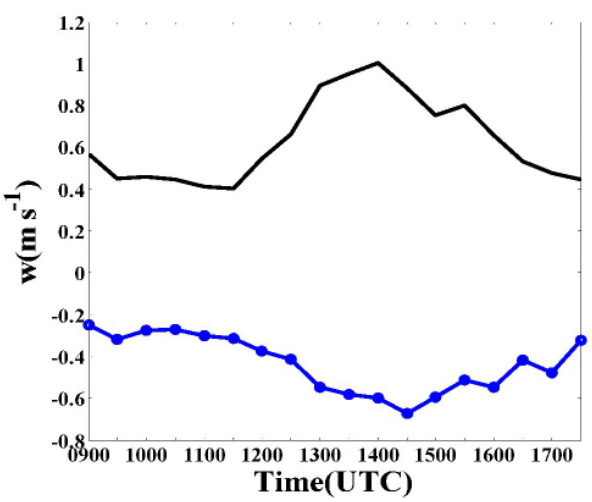

Figure 6. Average vertical velocity (units: m·s^{-1}) time evolution in the 800-hPa squall line area (black line for the time evolution of the average vertical velocity of updraft; the blue line for that of downdraft).

Within the study area, we follow the positions of the first 20 maxima of $\frac{\partial}{\partial t}\left(\frac{\partial \xi_y}{\partial x}-\frac{\partial \xi_x}{\partial y}\right)$, which were different at different times and at different levels. They were calculated based on the terms on the left hand side of the equation (these points were all located near the convection zone), to solve the averages of A, B, C, D, E, vlocc, and their sum. In order to determine the contribution of the terms on the right hand side of the horizontal vorticity equation, Fig.7 shows the temporal variations of these terms average on the aforementioned 20 maxima at each stage of the squall line evolution (see Fig.7).

From Fig.7, we can see that the term (vlocc) on the left hand side of the equation was not much different from the sum of all the terms on the right hand side, and their trends were almost the same, which also reflects the effectiveness of Eqs.(4) and (5). In Fig.7a, term A (vorticity caused by non-thermal wind) at 850 hPa was relatively small and fluctuated around zero; and from Eq.(6) we can see that it contributed little to the local change of vertical velocity. Term B (vorticity caused by horizontal advection) was significant in the later period and contributed much to the vertical movement but less from 1000 to 1300 UTC. Term C (vertical transport) was almost always positive and contributed most (especially in the development stage),

which was advantageous to the strengthening of the upward movement. Fig.7a also shows that, with the formation, development and maturity of the squall line, the magnitudes of A, B, C, vlocc, and sum would increase gradually and then become weaker with the weakening of the squall line. In Fig.7b, term A almost turned to be positive from zero at 500 hPa, namely, it contributed the most to vlocc. Term C, on the other hand, contributed the least to the variation, while term B was between A and C. Term A has the same trend as the sum; and in general, term A contributed the most at 500 hPa, which was advantageous to the development of the upward movement. Similar to the situation at 500 hPa, term A was the strongest at 200 hPa; term C contributed almost negatively; and term B stayed around the zero line. From Fig.7, at the mature stage of the squall line, term A contributed little to vlocc in the low-level atmosphere, while it contributed more and more with the increase of height and contributed most at 200 hPa, which was advantageous to the enhancement of upward movement. Term C contributed most in the low-level atmosphere, while it contributed less and less with the increase of the height and contributed least at 200 hPa, which could inhibit the upward movement. Term B contributed somewhere in between. Therefore, the quantitative analysis result shown in Fig.7 is consistent with that of the qualitative analysis in Fig.7.

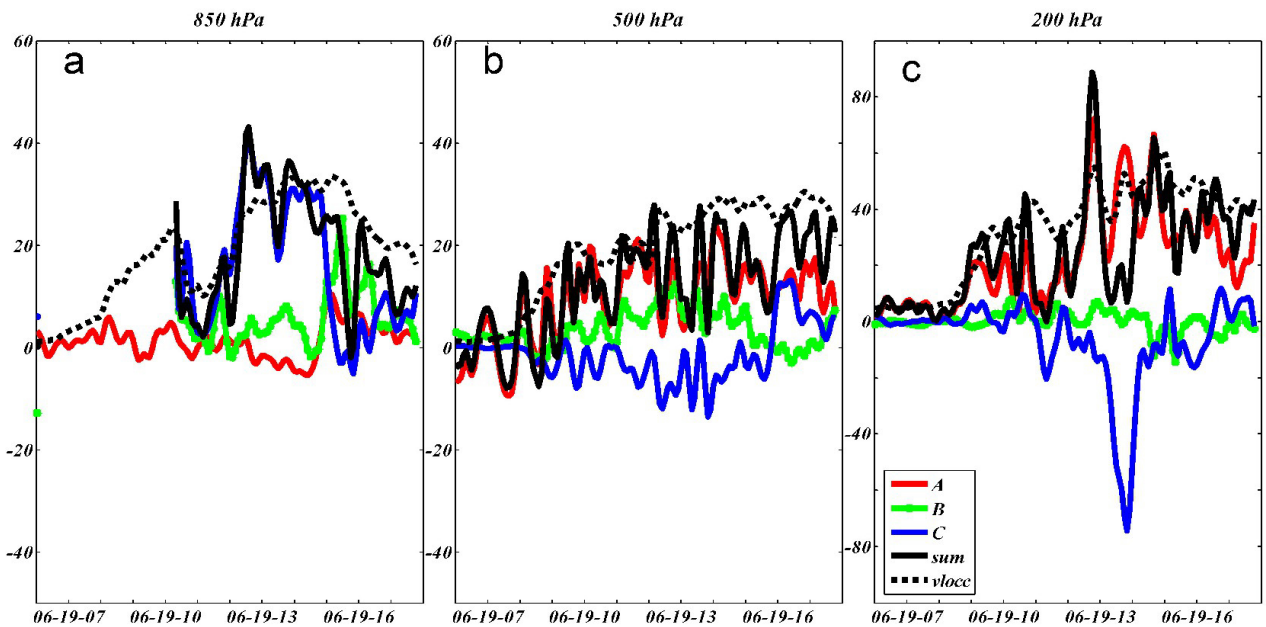

Figure 7. (a)-(c): The evolutions of A, B, C, vlocc and sum at 850, 500 and 200 hPa, respectively, from 0600 UTC to 1750 UTC on 19 June (units: 10^{-11}pa·s^{-2}).

Figure 8 shows the temporal evolutions of terms D and E from 0600 to 1750 UTC on 19 June. We can see that D and E were far smaller than C, B and A in terms of magnitude. At 800, 500 and 200 hPa, D and E were almost the same in magnitude but they contributed to the local change of vertical velocity in the opposite way.

In addition, as can be seen from Fig.8, terms D and E are obviously symmetrical about the zero line, which can be explained from the calculation of terms D and E. Term D indicates divergence, namely,

$$D=-\frac{\partial}{\partial x}\left(\frac{\partial v}{\partial y}\frac{\partial u}{\partial p}\right)-\frac{\partial}{\partial y}\left(\frac{\partial u}{\partial x}\frac{\partial v}{\partial p}\right)=-\frac{\partial^2 v}{\partial x\partial y}\frac{\partial u}{\partial p}-\frac{\partial v}{\partial y}\frac{\partial^2 u}{\partial x\partial p}-\frac{\partial^2 u}{\partial x\partial y}\frac{\partial v}{\partial p}-\frac{\partial u}{\partial x}\frac{\partial^2 v}{\partial y\partial p} \quad (7)$$

Let $m=-\frac{\partial^2 v}{\partial x\partial y}\frac{\partial u}{\partial p}-\frac{\partial^2 u}{\partial x\partial y}\frac{\partial v}{\partial p}$ and $n=-\frac{\partial v}{\partial y}\frac{\partial^2 u}{\partial x\partial p}-\frac{\partial u}{\partial x}\frac{\partial^2 v}{\partial y\partial p}$, then we get $D=m+n$. But term E is a twisting term, namely,

$$E=\frac{\partial}{\partial x}\left(\frac{\partial u}{\partial y}\frac{\partial v}{\partial p}\right)+\frac{\partial}{\partial y}\left(\frac{\partial v}{\partial x}\frac{\partial u}{\partial p}\right)=\frac{\partial^2 u}{\partial x\partial y}\frac{\partial v}{\partial p}+\frac{\partial u}{\partial y}\frac{\partial^2 v}{\partial x\partial y}+\frac{\partial^2 v}{\partial x\partial y}\frac{\partial u}{\partial p}+\frac{\partial v}{\partial x}\frac{\partial^2 u}{\partial x\partial y} \quad (8)$$

Let $m1=\frac{\partial^2 u}{\partial x\partial y}\frac{\partial v}{\partial p}+\frac{\partial^2 v}{\partial x\partial y}\frac{\partial u}{\partial p}$ and $n1=\frac{\partial u}{\partial y}\frac{\partial^2 v}{\partial x\partial p}+\frac{\partial v}{\partial x}\frac{\partial^2 u}{\partial y\partial p}$, then we get $E=m1+n1$.

Obviously, $m=-m1$. At the same time, u and v feature the same order of magnitude and act as the partial derivatives in the horizontal and vertical directions, so $|n|\approx|-n1|$. Consequently, D and E show certain symmetry but are not completely symmetric; because of these features, the contributions of D and E to the local change of vertical movement almost cancelled. Therefore, the contribution to the local change of vertical movement is mainly determined by A, B and C.

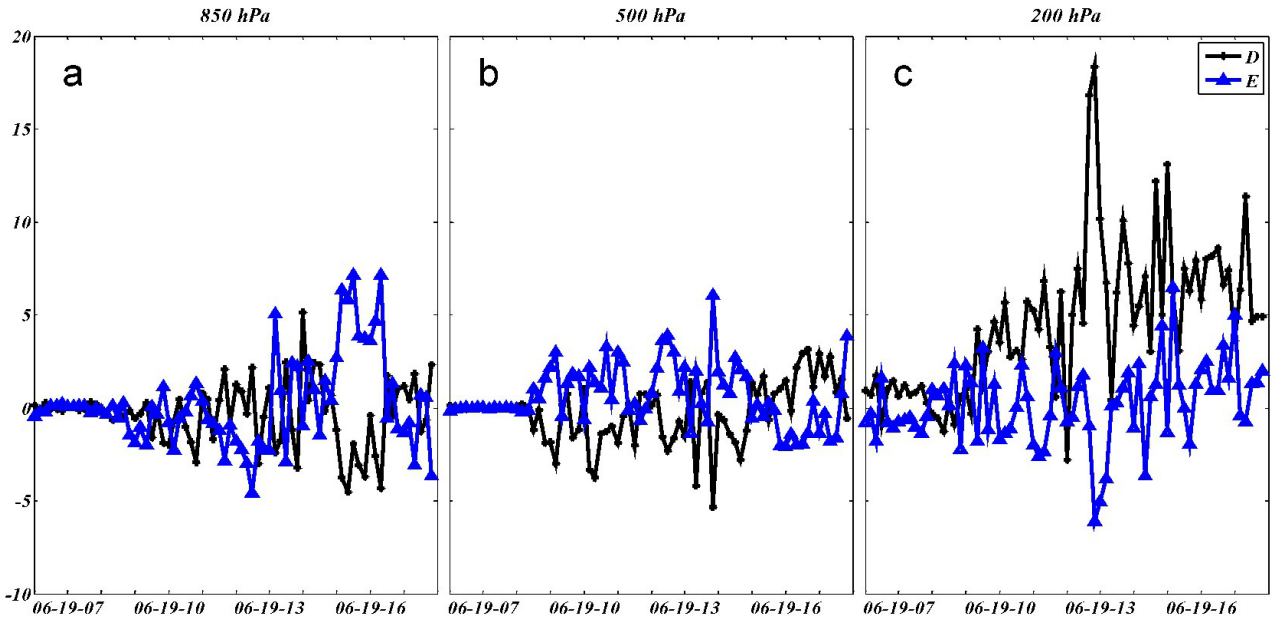

Figure 8. (a)-(c): Evolutions of D and E at 850, 500 and 200 hPa, respectively, from 0600 to 1750 UTC 19 June (units: 10^{-11} pa·s^{-2}).

In order to clearly reflect the vertical distributions of A, B, C, vlocc and sum, the time-averaged vertical distribution profiles are given for all the terms at four stages of the squall line: formation (0900−1050 UTC), development (1100−1350 UTC), maturity (1400−1550 UTC) and disappearance (1600−1750 UTC) (see Fig.9). In Fig.9, at various stages of the squall line evolution, term B changed less and always fluctuated near the zero line from the low-level atmosphere to the upper-level atmosphere; term A also changed slightly below 700 hPa but increased gradually with height above 700 hPa, and with the development and maturity of the squall line, the value of term A gradually increased but gradually decreased when the squall line started to disappear. As can be seen, in the mid- and upper-level atmosphere, term A was conducive to the strengthening of upward movement. From the early stage to the maturity stage, term C was characterized by a large positive value at 850 hPa, but the value decreased gradually upward at about 700 hPa to a negative value and to the maximum negative at 150 hPa. In the disappearance stage, term C changed slightly with height and was dominated by a positive value. From the low-level atmosphere to the upper-level atmosphere, vlocc and sum were consistent.

Figure 10 shows the meridional profiles of the latitudinal averages (i.e., latave_A, latave_C, latave_dBZ and latave_W) in the vicinity of the squall line for 1000, 1350, 1550 and 1650 UTC 800-hPa A, C, dBZ and W, respectively. The x-axis is the number of meridional lattice points. It can be seen from the figure, at 1000UTC, that is, the early formation of the squall line, radar echo reflectivity is weak, latave_A, latave_C and latave_W are also relatively weak. With the

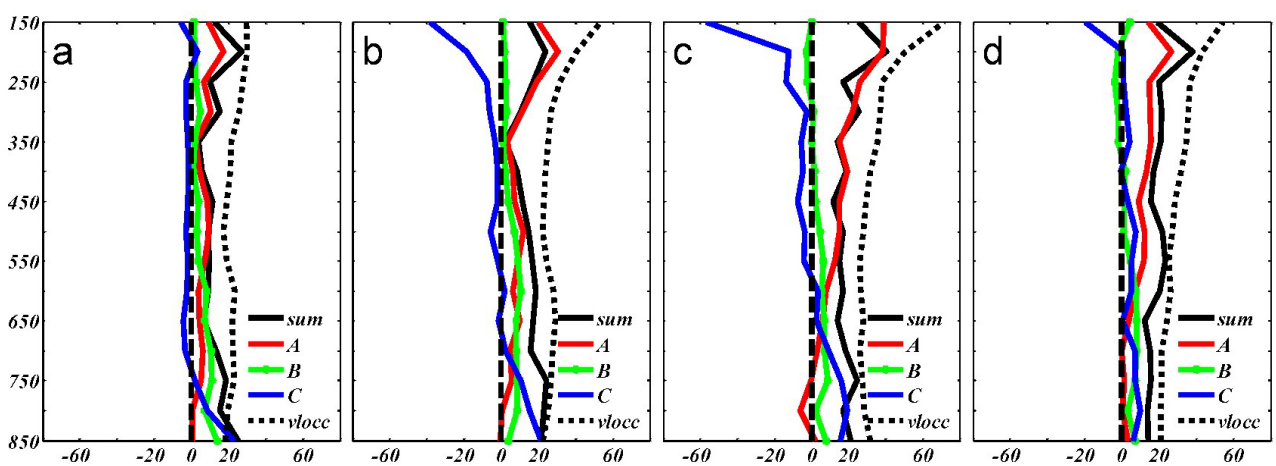

Figure 9. Time-averaged vertical profiles of terms A, B, C, vlocc and sum in different stages (x-axis units: 10^{-11} pa·s^{-2}; y-axis units: hPa): (a) 0900-1050 UTC; (b) 1100-1350 UTC; (c) 1400-1550 UTC; (d) 1600-1750 UTC.

development and maturity of the squall line, as shown in Fig.10b & 10c, latave_C and latave_W enhanced rapidly. At 1650UTC, as shown in Fig.10d, the squall line began to weaken, and latave_C and latave_W were rapidly weakening. The value of latave_A fluctuated little, which is consistent with the previous analysis, that is, the value for A is small at lower atmosphere. At the same time, it can be seen from Fig.10a-d that the peaks of latave_A and latave_C appear at the front of the squall line in the various stages of the squall line (especially the latave_A peak appears in the forefront). So these two terms on the evolution and direction of movement of squall line is somewhat indicative.

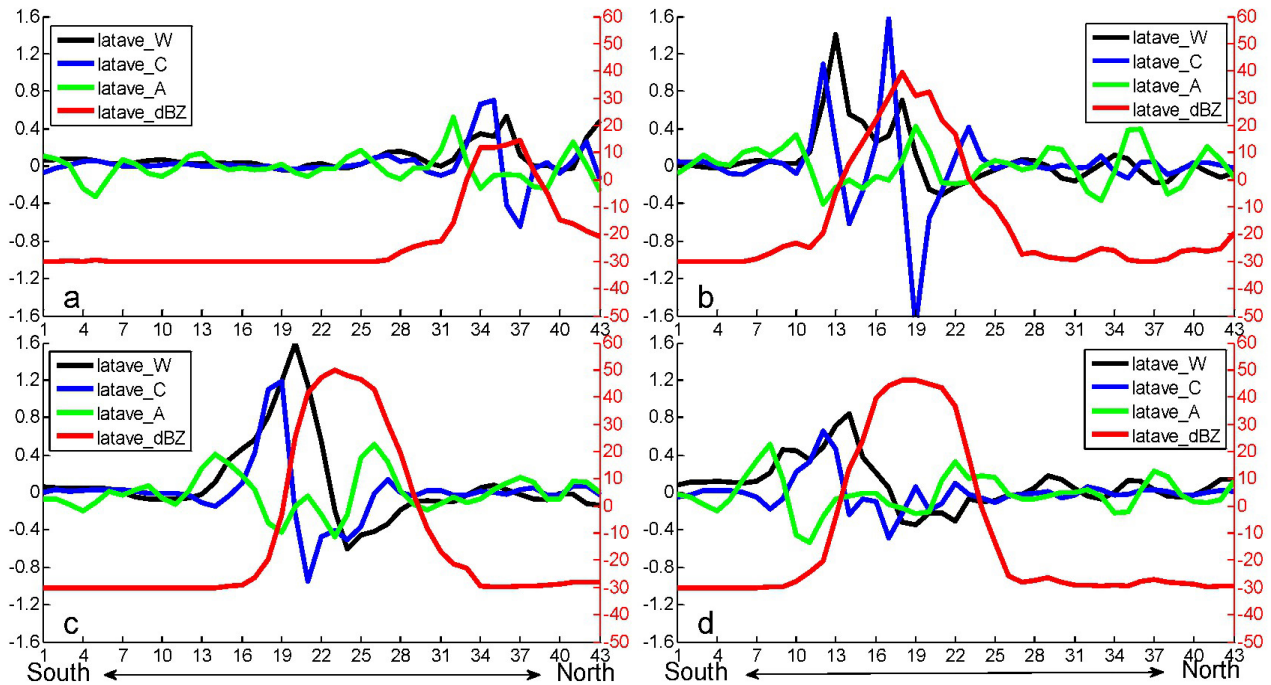

Figure 10. Meridional profiles of the latitudinal averages in the vicinity of the squall line for 800-hPa A, C, dBZ and W at (a) 1000 UTC, (b) 1350 UTC, (c) 1550 UTC and (d) 1650 UTC, respectively (latave_W: $m \cdot s^{-1}$; latave_A, latave_C: 10^{-10} $pa \cdot s^{-2}$, latave_dBZ: dBZ).

Why did term A (non-thermal wind term) have largest impact on the vertical movement in the mid- and upper-level atmosphere and term C (vertical transport term) contributed most in the low- and upper-level atmosphere, but their contributions were the opposite? The reasons will be discussed next.

5.3 *Analysis of the cause of the characteristic distribution*

5.3.1 ANALYSIS OF THE CAUSE FOR THE CHARACTERISTIC DISTRIBUTION OF THE VERTICAL TRANSPORT TERM

First, in order to explain the opposite impacts of term C on the vertical movement in the low-level atmosphere vs. the mid- and upper-level atmosphere, the time-averaged vertical distribution profiles are given for the vertical movement (w) and the magnitude of the horizontal vorticity vector (mhv) during the four stages of the squall line formation: (0900-1050 UTC), development (1100-1350 UTC), maturity (1400-1550 UTC), and disappearance(1600-1750 UTC) (see Fig.11).

Figure 11 shows that at each stage mhv rapidly decreased upward between 850 and 700 hPa, and rapidly increased upward between 250 and 150 hPa, while in the mid-level atmosphere, the mhv value was relatively smaller and changed little. Therefore, the mhv value changed significantly in the upper- and low-level atmosphere, with larger $\left|-\omega\frac{\partial\xi_y}{\partial p}\right|$ and $\left|-\omega\frac{\partial\xi_x}{\partial p}\right|$ transporting upward, because $\omega<0$. This kind of strong transportation of horizontal vorticity vector could easily cause stronger rotation of the horizontal vorticity vector, thus resulting in the distribution of term C seen in Fig.9. It also explains that the distributions of term C in the upper- and low-level atmosphere mainly resulted from the high-value zones of the two vertical wind shears in the upper- and low-level atmosphere, respectively. Especially, such distribution in the low-level atmosphere was conducive to the development of upward movement and the maintenance of the squall line, which is consistent with such conclusion that the stronger vertical shear in the low-level atmosphere is one of the important conditions for the occurrence of the squall line, as pointed out in most studies (Thorpe [20]; Blueestein, et al. [5, 6]). It also can be seen that, in the upper- and low-level atmosphere, mhv and vertical velocity increased along with the development and maturity of the squall line, but became weaker with the disappearance of the squall line.

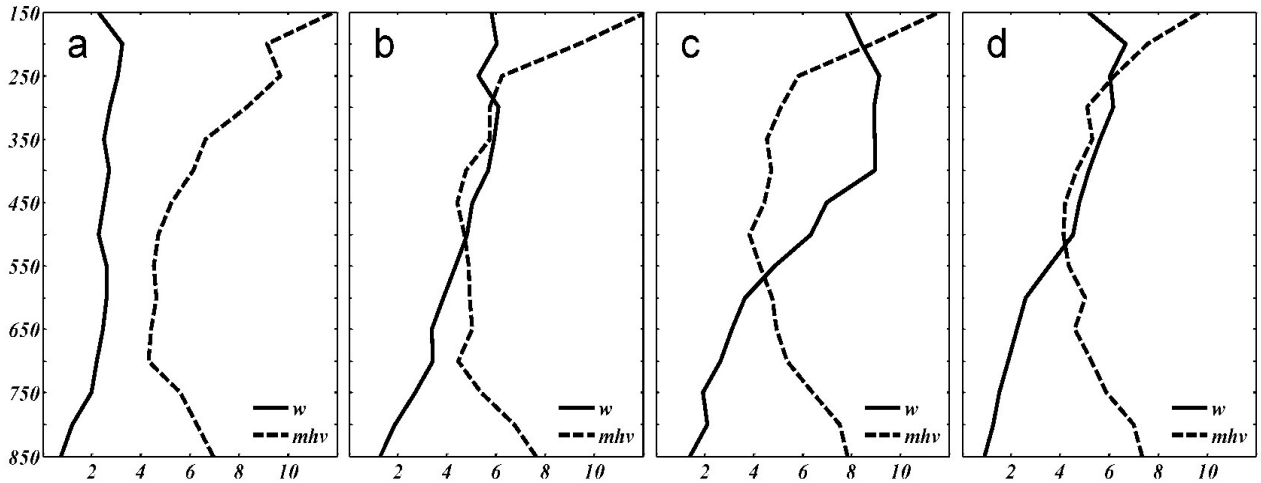

Figure 11. Time-averaged vertical distribution profiles for vertical motion, w (units: m·s^{-1}, solid line) and the magnitude of horizontal vorticity vector, mhv (units: 10^{-4} m^{-1}·s^{-1}·pa^{-1}; y-axis units: hPa) at the stages of (a) 0900–1050 UTC; (b) 1100–1350 UTC; (c) 1400–1550 UTC; and (d) 1600–1750 UTC.

5.3.2 ANALYSIS OF THE CAUSE FOR THE CHARACTERISTIC DISTRIBUTION OF THE NON-THERMAL WIND TERM

Here, we use the non-thermal wind vorticity, vertical movement and potential temperature to analyze the causes of the characteristics of non-thermal wind. The equation for non-thermal wind vorticity is:

$$\xi_{nt}=\frac{\partial v_{nt}}{\partial x}-\frac{\partial u_{nt}}{\partial y}=\frac{\partial}{\partial p}\left(\frac{\partial v'}{\partial x}-\frac{\partial u'}{\partial y}\right) \tag{9}$$

where ξ_{nt} is the non-thermal wind vorticity; u_{nt} and v_{nt} indicate the components of the non-thermal wind in the x and y directions, respectively; u' and v' indicate the ageostrophic winds ($u-u_g$, $v-v_g$), respectively; and $\frac{\partial v'}{\partial x}-\frac{\partial u'}{\partial y}$ represents the rotation of ageostrophic vector in the horizontal direction, hereinafter referred to as ageostrophic vorticity. Hence, it can be seen from Eq. (9) that the non-thermal wind vorticity equals to the change of ageostrophic vorticity with height. When the ageostrophic vorticity increased (decreased) with height, the non-thermal wind vorticity was positive (negative), and it was conductive to the enhancement of updraft (downdraft). Take a meridional cross section (Fig.12) along line AB in Fig.12d to show potential temperature, temperature, non-thermal wind vorticity, and vertical circulation fields and we can obtain such results as follows: when the high-altitude potential temperature surface was characterized by unapparent sinking, the non-thermal wind vorticity would be relatively weak in the potential temperature column (Fig.12a); when the potential temperature surface sank significantly, a clear warm air column (Fig.12b) would be formed in the mid- and upper-level atmosphere (the potential temperature surface subsidence caused by the condensation latent heating in most cases in this paper, not shown), the non-thermal wind vorticity increased quickly in the column and the corresponding vertical movement also became stronger. The above results show that when the potential temperature surface sank obviously with a warm air column coming into being, strong non-thermal wind vorticity would be produced, to further influence the upward movement in the mid- and upper-level atmosphere significantly. This would lead to imbalance of temperature field and air pressure field, and even form strong ageostrophic flow and ageostrophic vorticity.

According to the equations of motion:

$$\frac{du}{dt}=-g\frac{\partial H}{\partial x}+fv=f(v-v_g)=fv' \tag{10}$$

$$\frac{dv}{dt}=-g\frac{\partial H}{\partial y}-fu=-f(u-u_g)=-fu' \tag{11}$$

where H is the geopotential height. The ageostrophic vector is perpendicular to the horizontal acceleration vector and points to its left. The emergence of ageostrophic flow tends to cause change in horizontal acceleration, thus resulting in significant changes in horizontal wind and vertical shear.

We select 150 and 500 hPa as the upper- and lower-level atmosphere of the warm air column, respectively, and use Eqs.(10) and (11) to calculate the horizontal acceleration of the two convection layers for comparison with ageostrophic vorticity. The results show that at 1000 UTC 19 June when the potential temperature surface was lowered and formed a warm air column (Fig.12c & d), ageostrophic vorticity showed positive and negative centers, respectively, along with the warm cell centers at 150 and 500 hPa (ageostrophic vorticity increased with height, ageostrophic vector rotated clockwise at the lower level and counterclockwise at the upper level). The horizontal wind accelerations at upper and lower levels were characterized by obvious divergence and convergence,

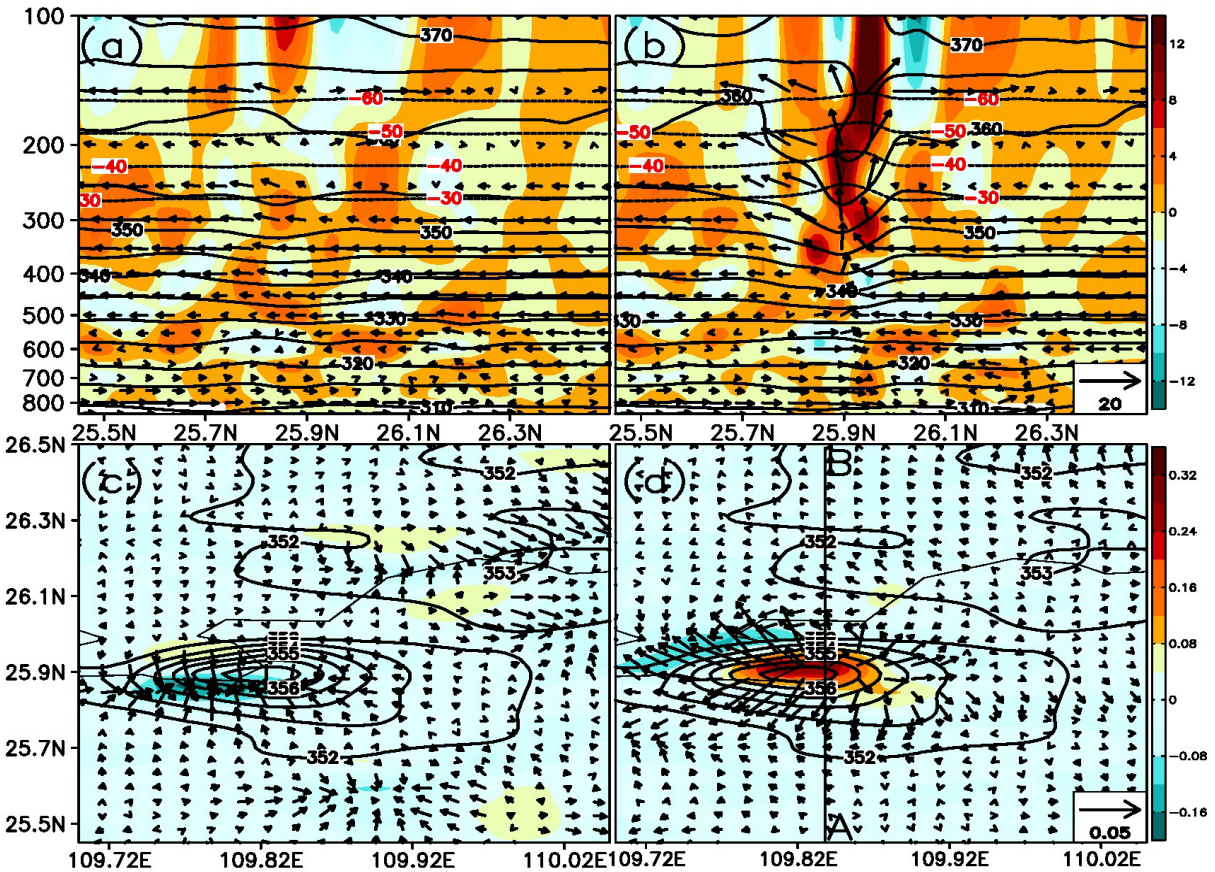

Figure 12. (a) and (b): Vertical sections (along line AB) of potential temperature (black contour; K), temperature (dotted black contour; ℃), non-thermal wind vorticity (shading; 10^{-5} $Pa^{-1}s^{-1}$), and vertical circulation (arrows; $m \cdot s^{-1}$) at 0950 and 1000 UTC, respectively. (c): 500-hPa horizontal acceleration (arrows; $m \cdot s^{-2}$), ageostrophic vorticity (shading; 10^{-5} $Pa^{-1}s^{-1}$) and 300-hPa potential temperature (contour; K) at 1000 UTC. (d): 150-hPa horizontal acceleration (arrow; $m \cdot s^{-2}$), ageostrophic vorticity (shading; 10^{-5} $Pa^{-1}s^{-1}$) and 300-hPa potential temperature (contour; K) at 1000 UTC.

respectively, which indicates that the ageostrophic vorticity enhancement with height in the warm air column tended to strengthen the divergence and convergence in the upper- and lower-level wind fields, respectively. This kind of phenomenon can cause horizontal vorticity increment pointing to the east at the south of the warm center from 500 to 150 hPa. Accordingly, in the east, north and west of the warm cell, horizontal vorticity increments would come into being, pointing to the north, west and south, respectively. As a result, this would cause cyclonic growth of horizontal vorticity and strengthening of upward movement (see Fig.13).

In conclusion, the formation of the mid- and upper-level warm air column induced by diabatic heating and the downward extension of potential temperature surface was the reason why term A was dominant in the mid- and upper-level atmosphere. The formation of the warm air column not only caused changes in wind field but also led to changes in horizontal vorticity and further resulted in changes in vertical movement.

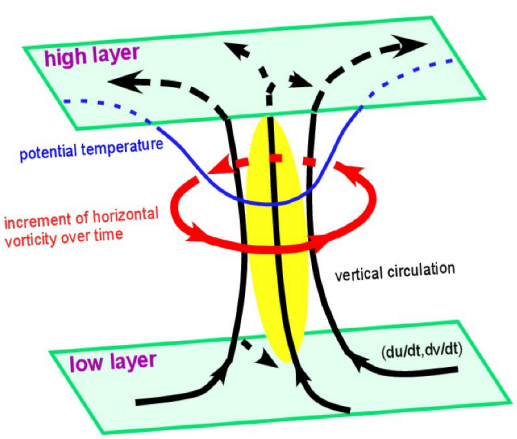

Figure 13. A conceptual model for the relationship between the non-thermal wind vorticity and vertical velocity. Yellow indicates the non-thermal wind vorticity area. The red vectors are the horizontal vorticity vectors induced by wind acceleration, the black vectors are for wind acceleration, the (solid and dotted) blue lines are contours for potential temperature, and the black vectors indicate the vertical circulation.

6 CONCLUSION AND DISCUSSION

Based on the numerical simulation of the squall line process on 19 June 2010 and diagnostic analysis of the horizontal vorticity induced by vertical shear, we draw the following conclusions.

(1) The horizontal vorticity, $(\xi_x, \xi_y) = \left(\frac{\partial v}{\partial p}, -\frac{\partial u}{\partial p}\right)$, induced by vertical shear and the horizontal vorticity equation can be derived from the equations of motion. The relative contribution of each term on the right hand side of the horizontal vorticity equation to the term $\left(\frac{\partial}{\partial t}\left(\frac{\partial \xi_y}{\partial x} - \frac{\partial \xi_x}{\partial y}\right) < -\frac{\partial \omega}{\partial t}\right)$ on the left hand side, namely, the local change of vertical velocity, can be seen through the vertical vorticity derived from each term in the horizontal vorticity equation.

(2) By calculating the 20 maximum points of $\frac{\partial}{\partial t}\left(\frac{\partial \xi_y}{\partial x} - \frac{\partial \xi_x}{\partial y}\right)$ along the convection belt, we found that non-thermal wind and vertical transport contributed more to the local change of vertical velocity, and the advection term contributed less. The twisting and divergence terms were one order of magnitude smaller than the others and both were basically symmetric; therefore, their contributions to the local change of vertical movement were basically cancelled.

(3) In the lower-level atmosphere, the non-thermal wind term had a small negative contribution to the local change of upward movement. Its contribution changed from negative to positive with the increase of height and simultaneously also increased with height. The vertical transport term was characterized by a positive contribution to the local change of upward movement in the low-level atmosphere, but the contribution changed from positive to negative up to the mid-level atmosphere and the negative contribution increased with height. The horizontal advection term basically contributed negatively to the local change of vertical movement, with the value smaller than the above-mentioned two terms.

(4) At each stage of the squall line, horizontal vorticity was unevenly distributed in the vertical direction, mainly characterized by stronger vertical wind shear in the upper- and lower-level atmosphere, thus resulting in violent changes of upward movement caused by vertical transport in the upper- and lower-level atmosphere, namely, it was conducive to the increase of upward movement in the lower-level atmosphere, while it could inhibit the upward movement in the upper-level atmosphere.

(5) At various stages of the squall line formation, development and maturity, the non-thermal wind term contributed less in the lower-level atmosphere, but its positive contribution gradually increased with height. At the stage of the strongest development of the squall line, the non-thermal wind term contributed most, mainly because in the process of the squall line evolution strong ageostrophic motion and uneven temperature and pressure fields occurred due to the sinking of potential temperature surface in the upper-level atmosphere, thus having strong horizontal acceleration convergence and divergence happening in the mid- and upper-level atmosphere, respectively. The change of the horizontal wind field could cause horizontal vorticity increment vector rotating counterclockwise around the warm cell, which generated an upward movement increment, namely, it could help strengthen the upward movement.

REFERENCES:

[1] NEWTON C W. Structure and mechanism of the prefrontal squall line [J]. J Meteor, 1950,7(3): 210-222.

[2] NEWTON C W. Circulations in large sheared cumulonimbus [J] . Tellus, 1963, 18(4): 699-713.

[3] FUJITA T T. Results of detailed synoptic studies of squall lines [J] . Tellus 1955, 7(4): 405-436.

[4] LUDLAM F H. Severe local storms: A review [J] //Atlas D. Meteor Monograph. Boston: American Meteor Society, 1963, 5(27): 1-30.

[5] BLUESTEIN H B, JAIN M H. Formation of mesoscale lines of precipitation: Severe squall lines in Oklahoma during the spring [J]. J Atmos Sci, 1985, 42 (16): 1711-1732.

[6] BLUESTEIN H B, MARX G T, JAIN M H. Formation of mesoscale lines of precipitation: Nonsevere squall lines in Oklahoma during the spring [J]. Mon Wea Rev, 1987, 115 (11): 2719-2727.

[7] ROTUNNO R, KLEMP J B, WEISMAN M L. A theory for strong long-lived squall lines [J]. J Atmos Sci, 1988, 45(3): 463-485.

[8] WEISMAN M L, KLEMP J B, ROTUNNO R. Structure and evolution of numerically simulated squall lines [J]. J Atmos Sci, 1988, 45(14): 1990-2013.

[9] WEISMAN M L, ROTUNNO R. "A theory for strong long-lived squall lines" revised [J]. J Atmos Sci, 2004, 61 (4): 361-382.

[10] WEISMAN M L, ROTUNNO R. Reply [J]. J Atmos Sci, 2005, 62(8): 2997-3002.

[11] BRYAN G H, KNIEVEL J C, PARKER M D. A multimodel assessment of RKW theory's relevance to squall-line characteristics [J]. Mon Wea Rev, 2006, 134 (10): 2772-2792.

[12] DING Zhi-ying, ZHAO Xiang-jun, GAO Song. A novel method for calculating vertical velocity: A relationship between horizontal vorticity and vertical movement [J]. J Trop Meteor, 2016, 22(2): 208-219.

[13] PARKER M D, JOHNSON R H. Organizational modes of midlatitude mesoscale convective systems [J]. Mon Wea Rev, 2000, 128(10): 3413-3436.

[14] WECKWERTH T M. The effect of small-scale moisture variability on thunderstorm initiation [J]. Mon Wea Rev, 2000, 128(12): 4017-4030.

[15] ROMANSKI J, ROSSOW W B. Contributions of individual atmospheric diabatic heating processes to the generation of available potential energy [J]. J Climate, 2013, 26(12): 4244-4263.

[16] PENG Jun, ZHANG Li-feng, LUO Yu, et al. Mesoscale energy spectra of the Mei-Yu front system. Part II: Moist available potential energy spectra [J]. J Atmos Sci, 2014, 71(4): 1410-1424.

[17] LIN Y L, FARLEY R D, ORVILLE H D. Bulk parameterization of the snow field in a cloud model [J]. J Climate Appl Meteor, 1983, 22: 1065-1092.

[18] NOH Y, CHEON W G, HONG S Y, et al. Improvement of the K-profile model for the planetary boundary layer based on large eddy simulation data [J]. Bound-Layer Meteor, 2003,107, 401-427.

[19] ZHU Qian-gen., LIN Jin-rui, SHOU Shao-wen, TANG Dong-sheng, Principles and Methods of synoptic Meteorology [M]. Beijing: China Meteorological Press, 2007 (in Chinese).

[20] THORPE A J, MILLER M J, MONCRIEFF M W. Two-dimensional convection in non-constant shear: A model of mid-latitude squall lines [J]. Quart J Roy Meteor Soc, 1982, 108(458): 739-762.

Citation: ZHAO Xiang-jun and DING Zhi-ying. The relationship between horizontal vorticity induced by vertical shear and vertical motion during a squall line process [J]. J Trop Meteor, 2018, 24(1): 1-14.